

# Dynamics of the quantum Duffing oscillator in the driving induced bistable regime<sup>?</sup>

V. Peano and M. Thorwart

Institut für Theoretische Physik IV, Heinrich-Heine-Universität Düsseldorf,  
Universitätsstr. 1, 40225 Düsseldorf, Germany

---

## Abstract

We investigate the nonlinear response of an anharmonic monostable quantum mechanical resonator to strong external periodic driving. The driving thereby induces an effective bistability in which resonant tunneling can be identified. Within the framework of a Floquet analysis, an effective Floquet-Born-Markovian master equation with time-independent coefficients can be established which can be solved straightforwardly. Various effects including resonant tunneling and multiphoton transitions will be described. Our model finds applications in nano-electromechanical devices such as vibrating suspended nano-wires as well as in non-destructive read-out procedures for superconducting quantum bits involving the nonlinear response of the read-out SQUID.

Key words: Quantum dissipation, tunneling, driven systems, nonlinear response  
PACS: 03.65.-w, 62.25.+g, 62.30.+d, 03.65.Xp

---

## 1 Introduction

Classical nonlinear systems subjected to strong periodic external driving often have several stable stationary states for which the amplitudes and phases of the forced vibrations differ in size [1,3]. One of the simplest theoretical models which show the coexistence of two stable states induced by external driving is the well-known classical Duffing oscillator. An anharmonic statically monostable potential can be driven into a dynamically bistable regime showing various interesting features of non-linear response [1,3], such as hysteresis,

---

<sup>?</sup> This work is dedicated to Prof. Phil Pechukas.

Corresponding author

Email address: thorwart@thphy.uni-duesseldorf.de (M. Thorwart).

period doubling, and thermal activation when finite temperatures are considered. The external driving field with frequency  $\omega$  induces an effective dynamic bistability which is manifest by the non-monotonous dependence of the amplitude  $A$  of the stationary vibrations for varying  $\omega$ . For the classical system where all potential energies are allowed, this response curve  $A(\omega)$  is smooth showing only two points of bifurcation for the related bistability. If the control parameter  $\omega$  is additionally varied adiabatically, hysteretical jumps between the two stable states occur. If additionally thermal noise is added to the system, the regime of bistability shrinks due to thermal escape of the metastable state.

The main subject of this work is to investigate the corresponding driven quantum mechanical system. The presence of time-dependent driving typically adds several interesting features to the properties of the time-independent quantum system, see for instance Refs. [4,5]. In this work, the focus is laid on the nonlinear response of the driven quantum mechanical anharmonic oscillator in the presence of an Ohmic heat bath. We show that the nonlinear response curve  $A(\omega)$  displays beyond its characteristic shape additional quantum mechanical resonances which are related to multiphoton absorptions. Additionally, we show that there exists a separation of time-scales indicating that the stationary state is reached by quantum tunneling from the dynamically induced metastable to the globally stable state. In fact, by tuning the control parameter  $\omega$ , several resonant tunneling transitions can be identified as resonances in the corresponding tunneling rate.

The paper is organized in the following way: In Section 2, the system Hamiltonian is introduced. The latter is periodic in time, which allows the application of Floquet theory. Since we are interested in the stationary state in presence of (weak) dissipation, we introduce also a set of harmonic oscillators representing an Ohmic heat bath. An efficient way to determine the dynamics of the system is the use of a Born-Markovian master equation in the Floquet picture (Section 3) yielding a simple master equation with time-independent rate coefficients. After straight forward diagonalization, the stationary oscillation amplitude  $A$  and the phase  $\phi$  follow. In Sections 4 and 5, the nonlinear response of  $A$  and  $\phi$  depending on the various parameters is studied in detail. In Section 6, resonant tunneling is investigated. Finally, in Section 7, we discuss the applicability of our model to experimental systems before we conclude.

## 2 The quantum Duffing oscillator

The Hamiltonian for the driven anharmonic oscillator has the form

$$H_S(t) = \frac{p^2}{2m} + \frac{m\omega_0^2}{2}x^2 + \frac{\gamma}{4}x^4 + x f \cos(\omega t) : \quad (1)$$

Here,  $m$  and  $\omega_0$  are the mass and the harmonic frequency of the resonator, respectively, while  $\lambda$  gives the strength of the nonlinearity. We focus on the case  $\lambda > 0$  of hard non-linearities, where the undriven potential is monostable. The external driving is characterized by the amplitude  $f$  and the frequency  $\omega$ . As it will become clear below, the driving induces an effective bistability in which quantum tunneling can be identified.

We include the effect of the environment by a bath of harmonic oscillators which are bilinearly coupled to the system with the coupling constants  $c_j$  [6]. The Hamiltonian for the bath and the coupling to the system is given by its standard form

$$H_B = \frac{1}{2} \sum_j \left( \frac{p_j^2}{m_j} + m_j \omega_j^2 x_j + \frac{c_j}{m_j \omega_j^2} x_j \right) \quad (2)$$

We focus on the generic case of an Ohmic bath with the spectral density

$$J(\omega) = \frac{\lambda^2}{2} \sum_j \frac{c_j^2}{m_j \omega_j} \delta(\omega - \omega_j) = m \gamma \omega e^{-\omega/\omega_c}; \quad (3)$$

with damping constant  $\gamma$  and cut-off frequency  $\omega_c$ . The total Hamiltonian is  $H(t) = H_S(t) + H_B$ .

To proceed, we scale  $H(t)$  to dimensionless quantities such that the energies are in units of  $\hbar\omega_0$  while the lengths are scaled in units of  $x_0 = \sqrt{\hbar/m\omega_0}$ . Put differently, we formally set  $m = \hbar = \omega_0 = 1$ . The nonlinearity parameter  $\lambda$  is scaled in units of  $x_0^4 = \hbar^2/\omega_0^2$ , while the driving amplitude is given in units of  $f_0 = \hbar\omega_0/x_0$ . Moreover, we scale temperature in units of  $T_0 = \hbar\omega_0/k_B$  while the damping strengths are measured with respect to  $\omega_0$ .

To investigate the dynamical behavior of the driven resonator, it is convenient to use the periodicity of  $H_S(t)$  with respect to time and switch to the Floquet picture [7], the latter being equivalent to a transformation to the rotating frame. The Floquet or quasienergies  $\epsilon$  follow from the solution of the eigenvalue equation

$$H_S(t) - i \frac{\partial}{\partial t} \sum_j |j(t)\rangle = \epsilon \sum_j |j(t)\rangle; \quad (4)$$

with the Floquet states  $|j(t)\rangle$ . The quasienergies  $\epsilon$  are defined up to a multiple integer of  $\omega$ , i.e., the state  $|j^{(n)}(t)\rangle = e^{in\omega t} |j(t)\rangle$  is also an eigenstate of the Floquet Hamiltonian, but with the eigenvalue  $\epsilon_n = \epsilon + n\omega$ . This feature prevents us from a global ordering of the quasienergies which, however, can be achieved with the mean energies obtained after averaging over

one driving period, i.e.,

$$\overline{E} = \sum_n (\omega_n + n\omega) \hbar c_{jn} \tilde{c}_{jn}; \quad (5)$$

with the Fourier components of the Floquet states [7]

$$\tilde{c}_{jn} = \frac{1}{2\pi} \int_0^{2\pi} dt e^{in\omega t} c_j(t); \quad (6)$$

### 3 Dynamics of the quantum Duffing oscillator

#### 3.1 Floquet-Born-Markovian master equation

The dynamics of the resonator in the regime of weak coupling to the bath can be efficiently described by a Born-Markovian master equation in the Floquet picture [7] for the elements  $\langle n | \rho(t) | j \rangle \langle j | \rho(t) | i \rangle$  of the reduced density operator after the harmonic bath has been traced out in the usual way. For weak damping, the dissipative influence of the bath is relevant only on a time scale much larger than the driving period  $T_d = 2\pi/\omega$ . Thus, the time-dependent coefficients which are periodic in time with period  $T_d$  can safely be replaced by their average over one driving period (moderate rotating wave approximation [7]). This yields a simplified master equation with time-independent coefficients which reads

$$\dot{\rho}_{jn}(t) = \sum_{k,l} M_{jn,kl} \rho_{kl}(t); \quad (7)$$

with

$$M_{jn,kl} = \frac{i}{\hbar} (\langle n | H | k \rangle \langle l | - \langle k | H | l \rangle \langle n |) + L_{jn,kl}; \quad (8)$$

The first term on the r.h.s. describes the coherent time evolution of the pure system while the second term contains the transition rates describing the influence of the dissipative bath. It reads [7]

$$L_{jn,kl} = \sum_n (\langle n | N | 0 \rangle + \langle n | N | 0 \rangle) X_{0n} X_{0n}^* \delta_{jn} + \sum_{\omega_n} \langle n | N | \omega_n \rangle X_{0\omega_n} X_{\omega_n,0}^* \delta_{jn} + \sum_{\omega_n} \langle n | N | \omega_n \rangle X_{0\omega_n} X_{\omega_n,0}^* \delta_{jn}; \quad (9)$$

with the coefficients

$$N_{\alpha} = N \left( \frac{1}{2} + \frac{1}{2} \frac{1}{e^{\beta \hbar \omega}} \right); \quad N(\omega) = \frac{1}{2} \frac{1}{e^{\beta \hbar \omega}}; \quad (10)$$

$$X_{\alpha} = \frac{1}{2} \int_0^{\infty} dt e^{-\lambda t} \langle x(t) x(0) \rangle; \quad (11)$$

The operator  $M$  in Eq. (8) is a  $M^2 \times M^2$  matrix, when the total Hilbert space of the anharmonic resonator has been truncated to the  $M$  dimensional subspace. For practical purposes, we set  $M = 12$  throughout this work. Note that we have confirmed convergence with respect to  $M$  for all results shown below. With that,  $M$  can be readily diagonalized numerically by standard means. This can be formalized in terms of the diagonalization transformation  $S$  by the eigenvalue equation

$$M S^{-1} = \Lambda S; \quad \Lambda_{\alpha\beta} = \delta_{\alpha\beta} \lambda_{\alpha}; \quad (11)$$

Here,  $\lambda_{\alpha}$  denote the eigenvalues of the operator  $M$ . Since the master equation (7) conserves the trace of  $\rho$ , there is an eigenvalue  $\lambda_1 = 0$  which characterizes the stationary solution  $\rho^{\text{st}}$ . The remaining eigenvalues all have a negative real part leading to a decay of the corresponding mode with time. Due to the structure of the master equation (7), there exist two classes of eigenvalues: (i) the first class having an imaginary part of zero consists of individual eigenvalues (associated to relaxation), and (ii) the second class having non-zero imaginary parts (associated to dephasing) consists of pairs of complex conjugated eigenvalues. The eigenvalues can be ordered according to the size of the absolute value of their real parts. As it turns out, there is one pair of complex conjugated eigenvalues, i.e.,  $\lambda_{\alpha}^{(1)} = \lambda_{\alpha}^{(2)*}$  with the smallest non-zero absolute value of the real part. Moreover, we find that that pair of eigenvalues is clearly separated in size from the remaining ones with respect to the real parts indicating a separation of time scales. That pair of eigenvalues is responsible for the tunneling dynamics at long times, as will be discussed in Section 6. Finally, the solution of the master equation (7) can be formally written as

$$\rho(t) = \rho^{\text{st}} + \sum_{\alpha \neq 1} S^{-1} \Lambda_{\alpha} e^{-\lambda_{\alpha} t} S \rho(0); \quad (12)$$

For convenience, we have chosen the initial time  $t = 0$ .

### 3.2 Observable: Stationary oscillation amplitude

We are interested in calculating the asymptotic expectation value  $\langle x \rangle_{t \rightarrow \infty}$  of the position operator. This is the quantity which can directly be compared to its classical counterpart being the solution of the classical Duffing equation.

It reads

$$x(t)_{\text{as}} = \sum_n c_n e^{in\omega t} \quad (13)$$

with the coefficients

$$c_n = A_n e^{i\phi_n} = \frac{1}{2\pi} \int_0^{2\pi} x(t)_{\text{as}} e^{-in\omega t} dt \quad (14)$$

Since the oscillator is driven by a cosine-shaped external force, it will oscillate in the asymptotic limit also with a phase-shifted cosine if the excitation frequency  $\omega$  remains close to  $\omega_0$ . Higher harmonics could be generated in this nonlinear system but they are not in the focus of our interest in this work. Thus, only the terms  $n = \pm 1$  contribute in the Fourier expansion and we obtain

$$x(t)_{\text{as}} = A \cos(\omega t + \phi); \quad \omega \approx \omega_0 \quad (15)$$

with the amplitude  $A = 2A_1$  and the phase  $\phi = \phi_1$  of the first harmonic of the Fourier expansion. These two quantities are used to study the nonlinear response of the anharmonic resonator in the stationary long-time limit. The short time dynamics of such a type of master equation is an interesting issue by itself since it is related to the question of complete positivity and to the question of factorizing initial conditions [8,9]. Moreover, we note that the master equation (7) is valid only in the case of weak system-bath coupling. For the opposite limit of strong coupling (quantum Smoluchowski limit), different techniques [10-14] have to be applied.

### 3.3 Classical Damped oscillator

The corresponding classical oscillator (at zero temperature) is the well-known Damped oscillator [13]. It shows a rich variety of features including regular and chaotic motion. In this work, we focus on the parameter regime where only regular motion occurs. The nonlinear response of its amplitude  $A$  can be calculated perturbatively [1]. One obtains the response  $A(\omega)$  as the solution of the equation

$$\omega - \omega_0 = \frac{3}{8m\omega_0} A^2 - \frac{f^2}{4m^2\omega_0^2 A^2} - \frac{\omega^2 - \omega_0^2}{4} A^4; \quad (16)$$

Its characteristic form is shown in the inset of Fig. 1. For weak driving strengths, the response as a function of the driving frequency  $\omega$  has the well-known form of the harmonic oscillator with the maximum at  $\omega = \omega_0$ . For increasing driving strength, the resonance grows and bends away from the

$\omega = \omega_0$ -axis towards larger frequencies (since  $\gamma > 0$ ). The locus of the maximum amplitudes is given by the parabola [1]  $\omega_0 = \frac{3}{8m\omega_0} A^2$ , which is often called the backbone curve. Most importantly, a bistability develops with two adjacent stable branches and one intermediate unstable branch. This bistability is connected with a hysteretical jump phenomenon which can be probed if the driving frequency  $\omega$  is adiabatically increased or decreased. The hysteresis is maximal for zero temperature. At finite temperature, it is reduced since the particle can escape from the metastable local minimum to the adjacent global minimum via thermally hopping [15{17}] before the deterministic switching point is reached [18,19]. Note that for stronger driving amplitudes, also bifurcations and period doublings can occur [13] which we do not address in the present work.

The nonlinear response of the phase  $\phi$  can be determined perturbatively in a similar way. One obtains [1]

$$\phi = \arctan \frac{A}{2((\omega - \omega_0)A - \frac{3}{8} \frac{A^3}{\omega_0})}; \quad (17)$$

where  $A$  is the solution of Eq. (16). The curve  $\phi(\omega)$  also has two stable branches with an unstable intermediate branch and displays similar hysteretical jump phenomena as the amplitude response.

As we will show in the following, the nonlinear response is qualitatively different in the corresponding quantum system. The discrete quasi-energy spectrum allows for multi-photon excitations which yield discrete resonances in the amplitude response profile. Moreover, the dynamically generated bistability allows for an escape of the system out of the metastable state via resonant quantum tunneling. This generates characteristic resonances in the tunneling rate when the external frequency  $\omega$ , which plays the role of a control parameter, is tuned.

#### 4 Amplitude response

A typical response profile for the amplitude  $A(\omega)$  is shown in Fig. 1. The shoulder-like shape is a remnant of the classical form of the response which is indicated by the dashed line. In the quantum case, clear resonances can be observed at particular values of the driving frequency.

The resonances can be understood as discrete multi-photon transitions occurring when the  $N$ -th multiple of the field quantum  $\sim \omega$  equals the corresponding energy gap in the anharmonic oscillator. By inspection of the associated quasienergy spectrum shown in Fig. 2, one can see that the distinct reso-

nances occur at multiple degenerate avoided level crossings of the quasienergy level  $\epsilon_N$  of the  $N$ -th Floquet state with the quasienergy level  $\epsilon_0$  of the Floquet groundstate. In physical terms, multi-photon excitations occur in the resonator and the corresponding populated Floquet state dominates then the position expectation value  $\langle x \rangle$  with its large value of the amplitude, see Eqs. (13,14).

The width of the  $N$ -th resonance is determined by the minimal splitting at the avoided quasienergy level crossing which is equal to the  $N$ -photon Rabi frequency. The latter can be evaluated perturbatively for weak driving amplitudes [20,21] upon applying a rotating-wave approximation (RWA). For the resulting Hamiltonian, one finds that to lowest order in  $f = (\hbar \Omega_N / 2)$ , the  $N$ -photon Rabi frequency at  $\epsilon_N$  decreases exponentially with  $N$  implying that the resonances are sharper for larger  $N$ . For small frequencies, the broad peaks overlap strongly and lead to a shoulder-like profile which is similar to the classical result (dashed line in Fig. 1). Although the RWA yields a qualitatively correct picture, a quantitative comparison shows noticeable deviations from the results for the full anharmonic resonator and is not pursued further in this work. Note that a similar system has been investigated in Ref. [22] in the context of a dispersive optical bistability. There, a nonlinear Hamiltonian has been derived from the Duffing oscillator using a RWA, similar to that used in Ref. [23,20]. A rather involved matrix continued-fraction method also revealed a bistability. However, the numerical procedure to obtain those results is rather cumbersome. In contrast, our approach is numerically straightforward since it only involves a simple numerical diagonalization of a matrix.

#### 4.1 Tuning system parameters

Since the location of the multi-photon resonances is determined by the system Hamiltonian, it is interesting to see how they depend on varying the system parameters  $\gamma$  and  $f$ .

##### 4.1.1 Varying the nonlinearity coefficient

The spectrum of the system and therefore, the Floquet spectrum, depends strongly on the nonlinearity coefficient  $\gamma$ . Increasing  $\gamma$  increases the energy gaps between the succeeding eigenstates. Thus, the multiphoton absorption processes occur at larger frequencies of the driving field. This behavior is shown in Fig. 3. The increase of  $\gamma$  leads in general to a shift of the response curve  $A(\Omega)$  towards larger frequencies  $\Omega$ . Moreover, we observe that the height of the  $N$ -photon peak decreases for increasing  $\gamma$ . This observation is qualitatively in agreement with a perturbative treatment for weak driving within a rotating



wave approximation [20].

#### 4.1.2 Varying the driving amplitude $f$ : $M$ -photon antiresonance

The Floquet spectrum of the uncoupled system depends on the value of the driving amplitude  $f$ . A perturbative analysis [20] shows that the  $N$ -photon Rabi frequency  $\omega_{R,N}$  which is given by the minimum splitting of the quasienergy at the avoided quasienergy level crossing depends crucially on  $N$  and  $f$ . This, in turn, determines the behavior of the  $N$ -photon resonance. The detailed results of the dependence on the  $f$  are shown in Fig. 4. The  $N = 5$ -photon peak grows for growing  $f$ . Most interestingly, the  $N = 6$ -photon peak displays a nontrivial behavior. For weak driving, a 6-photon antiresonance, i.e., a dip, develops. When the field amplitude is increased the antiresonance turns into a true resonance which grows further for growing  $f$ . The particular dependence of the local extrema are shown in the inset of Fig. 4. As follows from Eqs. (13) and (14), the amplitude  $A$  is determined by the sum  $c_1 = \sum_P^{N-1} X_{P,1}$ . Thus, the product of the weights  $c_1$  (which also contains the influence of the bath) and the matrix elements  $X_{P,1}$  (which is a property of the coherent driven system alone) determines the full shape of the amplitude. Notice that  $c_1$  is in general not diagonal. This is different from the system considered in Ref. [20] where only a coherent system without bath has been investigated.

By varying the system parameters, we have modified implicitly both  $c_1$  and  $X_{P,1}$ . In the following section, only bath parameters and thus  $c_1$  will be modified, leaving  $X_{P,1}$  unchanged.

### 4.2 Dependence on bath parameters

The crossover from antiresonant to resonant behavior occurs when an increased driving amplitude  $f$  increases the population of higher-lying Floquet states. In this subsection, we investigate the role of the dissipative environment by tuning the bath temperature and the damping constant.

#### 4.2.1 Varying temperature $T$

Since increasing temperature  $T$  leads also to an increased population of other Floquet modes, the transition from antiresonant to resonant behavior can also be expected to occur for growing  $T$ , at least in a certain temperature regime. The result is shown in Fig. 5 for the 5-photon and 6-photon-resonance. The resonant peak for  $N = 5$  grows and broadens if temperature is increased. In contrast, the antiresonant dip for  $N = 6$  shrinks for growing  $T$  and turns into a resonant peak. This peculiar behavior can be interpreted as thermally

assisted cross-over from antiresonant to resonant behavior. The inset in Fig. 5 shows the local extrema for  $N = 5$  and  $N = 6$ . For even larger temperature  $k_B T \sim \hbar\omega_0$ , the characteristic peak structure is completely smeared out due to thermal broadening, see also Fig. 2, lower panel. Then, the peaks overlap and the dynamic bistability is smeared out by thermal transitions between the two (meta-)stable states.

#### 4.2.2 Varying the damping constant

The results for different damping constants are shown in Fig. 6. The five-photon resonance decreases when  $\gamma$  is increased from  $\gamma = 0.001\hbar\omega_0$  to  $\gamma = 0.01\hbar\omega_0$ . As also shown in the inset of Fig. 6, the peak maximum decreases monotonously for  $N = 5$ . For the six-photon (anti-)resonance, we find a different behavior. For weak damping, a sharp resonance occurs which is turned into an antiresonance for larger damping. The non-monotonous dependence of the six-photon resonance is also shown in the inset of Fig. 6. As it is the case for very large temperature (see above), the influence of a strong coupling to the bath gradually smears out and finally destroys the resonances.

### 5 Phase response

Next, we address the nonlinear response of the phase  $\phi$ . The corresponding classical Duffing oscillator shows an interesting nonlinear phase response  $\phi(\omega)$  including two stable branches [1]. The characteristic multi-photon transitions in the quantum version of the Duffing oscillator also show up in the phase response profile. The results for different driving strengths  $f$  are shown in Fig. 7 for the regime where the five- and six-photon transition occur. For  $\omega < \omega_0$  a phase shift  $\phi = \pi$  is found. For  $\omega = \omega_0$ , the phase shift vanishes,  $\phi = 0$ . In the intermediate region  $\omega \approx \omega_0$ , the multi-photon resonances induce also an antiresonance in the phase shift. The five-photon antiresonance is enhanced and broadened if the driving strength  $f$  is increased from  $f = 0.09f_0$  to  $f = 0.1f_0$ . Increasing the driving further to  $f = 0.11f_0$  wipes out the antiresonance completely and the transition  $\phi = \pi$  to  $\phi = 0$  is shifted to larger values of  $\omega$ , where this development is repeated at the succeeding six-photon resonance.

This behavior is also found when temperature is varied, see Fig. 8. Increasing  $T$  leads to a suppression of the transition of the phase shift  $\phi = \pi$  to  $\phi = 0$ . In contrast, increasing damping favors this transition at lower frequencies  $\omega$ , see Fig. 9.

## 6 Resonant tunneling in the driving induced bistability

The dynamic bistability of the steady state of the classical Duffing oscillator does not survive in the quantum system. The reason is that the system will escape the metastable state asymptotically via tunneling, similar to the case of the driven double-well potential [24]. Note also that, as a consequence, the hysteretical behavior is suppressed if the control parameter  $\lambda$  is varied truly adiabatically.

Nevertheless, signatures of the dynamic bistability and tunneling can be found if we consider how the steady state is reached. For this, we show in Fig. 10 the time evolution of the amplitude  $A$  (local maxima of the vibrations) starting with the ground state of the undriven oscillator as the initial state. We observe fast oscillations at short times. They decay on a time scale  $\tau^{-1}$  which reflects "intrawell" relaxation in the metastable state. Then, starting from a metastable state at intermediate times, a slow exponential decay towards the asymptotically globally stable state can be observed. This separation of time scales is a clear indication of tunneling from the meta- to the globally stable in the dynamic bistability.

The decay rate  $\tau$  for this slow process (tunneling rate) is determined by the absolute value of the real part of the eigenvalue  $\lambda_{m, in}^{(1,2)}$  of the operator  $M$  in Eq. (8), i.e.,  $\tau = \text{Re}[\lambda_{m, in}^{(1,2)}]$ . Results for the tunneling rate as function of the control parameter  $\lambda$  are shown in Fig. 11 for two different damping constants  $\gamma$ . Most importantly, the tunneling rate shows resonances at the same values of the frequencies where the avoided crossings of the quasienergy levels occur (see dashed vertical lines). The peaks in  $\tau$  indicate resonant tunneling [24] from the meta- to the globally stable state both of which are dynamically induced. Note the analogy to resonant tunneling in a static double-well potential [24]. The role of the eigenenergies in the static case is now played by the quasienergies  $\epsilon$  determining the coherent dynamics, see Eq. (7). In both cases, the avoided (quasi-)energy level crossings are the origin of resonant tunneling. Nevertheless, the incoherent part of Eq. (7) is crucial to observe the resonant tunneling in this driving induced bistability.

Furthermore, it is interesting to note that the resonant tunneling is enhanced if the coupling to the bath is increased from  $\gamma = 0.001\gamma_0$  to  $\gamma = 0.005\gamma_0$  (bath assisted resonant tunneling). We have also calculated the dependence of this phenomenon on temperature but we found a weak dependence in the interesting low-temperature regime (not shown).

## 7 Discussion and conclusions

The quantum Duffing oscillator is a generic theoretical model which finds several applications in experimental systems. For instance, a suspended nanomechanical beam [25,26] which is excited to transverse vibrations behaves as a damped anharmonic resonator. Several experimental groups have observed the behavior described by the classical Duffing oscillator [27-30]. The transition to the quantum regime is currently in the focus of intense research [31-36]. Once, such kind of truly quantum ‘mechanical’ systems on the nanoscale have been shown to exist, macroscopic quantum effects [33] should be readily observable. A second class of experimental systems addresses the resonant non-destructive read-out of a persistent current qubit [37-40]. In contrast to the conventional switching current measurement that generates unwanted quasi-particles when the dc-SQUID (acting as the qubit detector) switches to the voltage state, this technique keeps the SQUID biased along the supercurrent branch during the measurement. Thereby, the Josephson plasma resonance of the SQUID depends on the inductive coupling of the SQUID to the qubit. Measuring the plasma resonance allows to non-destructively read out the qubit state. The application of this read-out technique in the nonlinear regime of the SQUID could allow for an improved sensitivity as well as its potential use as a nonlinear amplifier. Finally, we note that there exists a wide parameter regime (typically strong driving and/or big nonlinearities) where a quantum chaotic behavior of the system with many interesting features can occur [41,42]. A detailed study of this regime goes beyond the scope of this work.

To summarize, we have investigated the nonlinear response of the amplitude as well as of the phase of the oscillations of a driven damped anharmonic resonator (quantum Duffing oscillator). The use of an efficient Floquet-Bomarkovian master equation allows to determine the stationary long-time solution directly via straightforward diagonalization of the rate matrix. This allows to study the amplitude as well as the phase response for a wide range of parameters. Most importantly, we find pronounced resonances as well as antiresonances which are associated to multiphoton transitions in the resonator. We have found an interesting non-monotonous behavior of the antiresonance including a cross-over to a true resonant peak. This cross-over can be enhanced by the presence of the bath but is already inherent in the underlying coherent driven quantum system. Furthermore, we have found a clear separation of time scales in the dynamics how the globally stable state is approached starting from the metastable state. This tunneling process can be characterized by a single tunneling rate which follows straightforwardly as the smallest non-zero eigenvalue of the rate matrix. If the control parameter being the frequency  $\omega$  is varied, resonant tunneling between the two states clearly is discerned as peaks in the tunneling rate. We hope that these rich features of the quantum Duffing oscillator will be found in future experiments.

## 8 Acknowledgments

We are grateful to H. Postma for interesting discussions on suspended carbon nanotubes. This work has been supported by the German DFG SFB/TR 12.

## References

- [1] A. H. Nayfeh and D. T. Mook, *Nonlinear Oscillations* (Wiley, New York, 1979).
- [2] J. Guckenheimer and Ph. Holmes, *Nonlinear oscillations, dynamical systems, and bifurcations of vector fields* (Springer, New York, 1983).
- [3] E. A. Jackson, *Perspectives of nonlinear dynamics* (Cambridge UP, Cambridge 1991).
- [4] J. P. Davis and Ph. Pechukas, *J. Chem. Phys.* **64**, 3129 (1976).
- [5] Special Issue on Dynamics of Driven Quantum Systems, ed. by W. Domcke, P. Hanggi, and D. Tannor, *Chem. Phys.* **217**, 117-416 (1997).
- [6] U. Weiss, *Quantum Dissipative Systems* (World Scientific, Singapore, 2nd ed., 1999).
- [7] S. Kohler, T. Dittrich, and P. Hanggi, *Phys. Rev. E* **55**, 300 (1997).
- [8] Ph. Pechukas, *Phys. Rev. Lett.* **73**, 1060 (1994).
- [9] J. Ankerhold, M. Saltzer, and E. Pollak, *J. Chem. Phys.* **116**, 5925 (2002).
- [10] M. Thorwart and P. Jung, *Phys. Rev. Lett.* **78**, 2503 (1997).
- [11] M. Thorwart, M. Grifoni, and P. Hanggi, *Phys. Rev. Lett.* **85**, 860 (2000); *Ann. Phys. (N.Y.)* **293**, 15 (2001).
- [12] J. Ankerhold, Ph. Pechukas, and H. Grabert, *Phys. Rev. Lett.* **87**, 086802 (2001).
- [13] Ph. Pechukas, J. Ankerhold, H. Grabert, *J. Phys. Chem. B* **105**, 6638 (2001).
- [14] L. Machura, M. Kostur, P. Hanggi, P. Talkner, and J. Luczka, *Phys. Rev. E* **70**, 031107 (2004).
- [15] Ph. Pechukas, *Ann. Rev. Phys. Chem.* **32**, 159 (1981).
- [16] E. Pollak, H. Grabert, and P. Hanggi, *J. Chem. Phys.* **91**, 4073 (1989).
- [17] P. Hanggi, P. Talkner, and M. Borkovec, *Rev. Mod. Phys.* **62**, 251 (1990).
- [18] M. I. Dykman and M. A. Krivoglaз, *Sov. Phy. JETP* **50**, 30 (1979).
- [19] S. Datta and J. K. Bhattacharjee, *Phys. Lett. A* **283**, 323 (2001).

- [20] M . I . D yk m a n and M . V . F i s t u l , Phys. Rev. B 71, 140508 (R) (2005).
- [21] D . M . L a r s e n and N . B l o m b e r g e n , Opt. Com m . 17, 254 (1976).
- [22] K . V o g e l and H . R i s k e n , Phys. Rev. A 38, 2409 (1988).
- [23] M . I . D yk m a n and V . N . S m e l y a n s k i i , Sov. Phys. JET P 67, 1769 (1988).
- [24] M . T h o r w a r t , P . R e i m a n n , P . J u n g and R . F . F o x , Phys. Lett. A 239, 233 (1998); Chem . Phys. 235, 61 (1998).
- [25] M . L . R o u k e s , Physics W o r l d 14, 25 (2001); H . G . C r a i g h e a d , Science 290, 1532 (2000); A . N . C l e l a n d , Foundations of N a n o m e c h a n i c s , (Berlin, Springer, 2003).
- [26] A . N . C l e l a n d and M . L . R o u k e s , Appl. Phys. Lett. 69, 2653 (1996); A . N . C l e l a n d and M . L . R o u k e s , Nature 392, 161 (1998).
- [27] H . K r o m m e r , A . E r b e , A . T i l k e , S . M a n u s and R . H . B l i c k , Europhys. Lett. 50, 101 (2000).
- [28] A . E r b e , H . K r o m m e r , A . K r a u s , R . H . B l i c k , G . C o r s o and K . R i c h t e r , Appl. Phys. Lett. 77, 3102 (2000).
- [29] E . B u k s and M . L . R o u k e s , Europhys. Lett. 54, 220 (2001).
- [30] A . H u s a i n , J . H o n e , H . W . C h . P o s t m a , X . M . H . H u a n g , T . D r a k e , M . B a r b i c , A . S c h e r e r , and M . L . R o u k e s , Appl. Phys. Lett. 83, 1240 (2003).
- [31] S . M . C a r r , W . E . L a w r e n c e and M . N . W y b o u m e , Phys. Rev. B 64, 220101 (2001).
- [32] P . W e m e r and W . Z w e r g e r , Europhys. Lett. 65, 158 (2004).
- [33] V . P e a n o and M . T h o r w a r t , Phys. Rev. B 70, 235401 (2004).
- [34] X . M . H . H u a n g , C . A . Z o r m a n , M . M e h r e g a n y and M . R o u k e s , Nature 421, 496 (2003).
- [35] R . G . K n o b e l and A . N . C l e l a n d , Nature 424, 291 (2003).
- [36] M . D . L a H a y e , O . B u u , B . C a m a r o t a , and K . S c h w a b , Science 304, 74 (2004).
- [37] A . L u p a s c u , C . J . M . V e r w i j s , R . N . S c h o u t e n , C . J . P . M . H a m a n s , and J . E . M o o i j , Phys. Rev. Lett. 93, 177006 (2004).
- [38] P . B e r t e t , I . C h i o r e s c u , C . P . J . H a m a n s , and J . E . M o o i j , Phys. Rev. B 70, 100501 (R) (2004).
- [39] J . C . L e e , W . D . O l i v e r , T . P . O r l a n d o , and K . K . B e r g g r e n , cond-m at/0501283.
- [40] I . S i d d i q i , R . V i j a y , F . P i e r r e , C . M . W i l s o n , L . F r u n z i o , M . M e t c a l f e , C . R i g e t t i , R . J . S c h o e l k o p f , M . H . D e v o r e t , D . V i o n , and D . E s t e v e , Phys. Rev. Lett. 94, 027005 (2005).
- [41] P h . P e c h u k a s , J . P h y s . C h e m . 86, 2239 (1982).

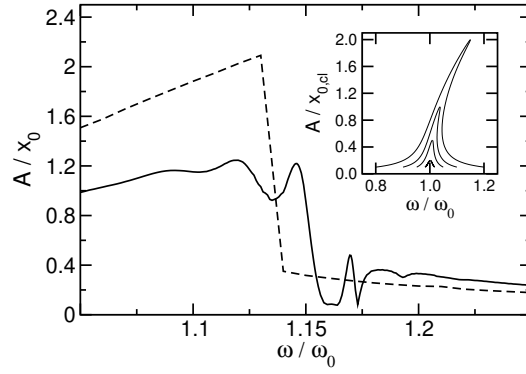


Fig. 1. Amplitude  $A$  of the expectation value  $\langle x(t) \rangle$  in units of  $x_0 = \sqrt{\frac{\hbar}{m\omega_0}}$  for varying the driving frequency  $\omega$ . Parameters are  $k_B T = 0.1\hbar\omega_0$ ;  $\gamma = 0.1\omega_0$ ;  $f = 0.1f_0$ ;  $\alpha = 0.005\hbar\omega_0$ . Dashed line: Results of the classical Duffing oscillator at  $T = 0$  with the remaining parameters being the same. Inset: Amplitude  $A$  of the classical Duffing oscillator for varying driving frequencies. The driving strength  $f$  increases from bottom to top.

[42] Ph. Pechukas, J. Phys. Chem. 88, 4823 (1984).

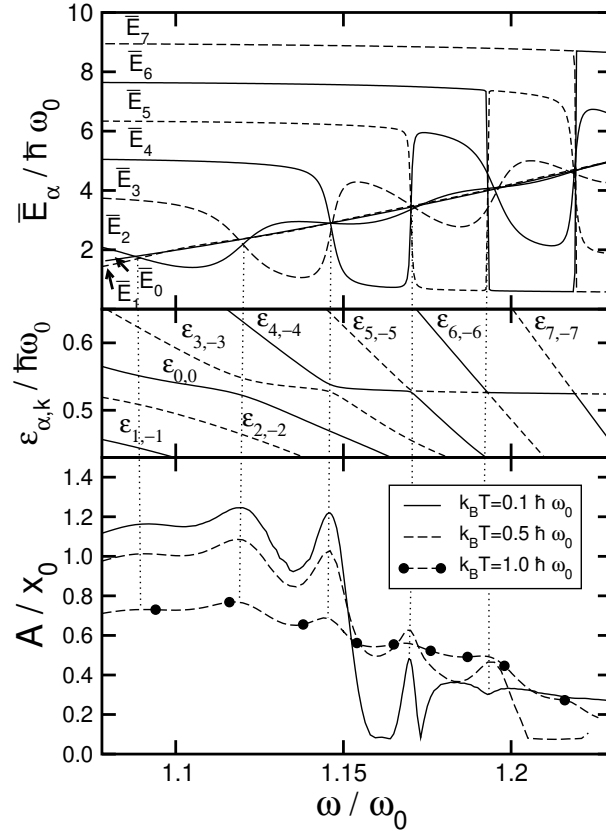


Fig. 2. Average energies  $\bar{E}_\alpha$  (top), quasienergy levels  $\varepsilon_{\alpha,k}$  (middle) and amplitude  $A$  of the fundamental mode for varying driving frequencies  $\omega$ . The remaining parameters are  $\gamma = 0.1 \omega_0$ ;  $f = 0.1 f_0$  and  $\delta = 0.005 \omega_0$ .



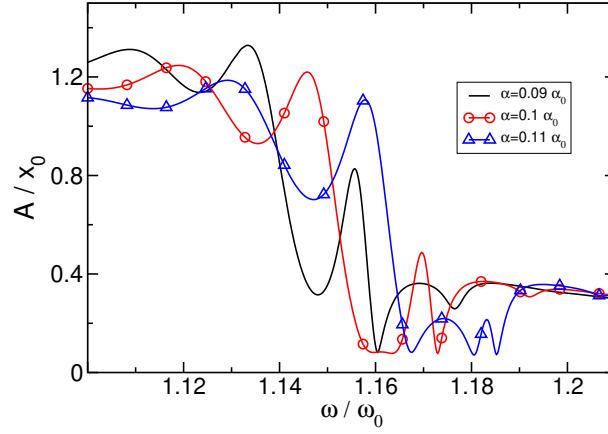


Fig. 3. (Color online) Response curve  $A(x_0)$  for different values of the nonlinearity. Remaining parameters are  $k_B T = 0.1 \sim 1_0$ ;  $f = 0.1 f_0$ ;  $\gamma = 0.005 \sim 1_0$ .

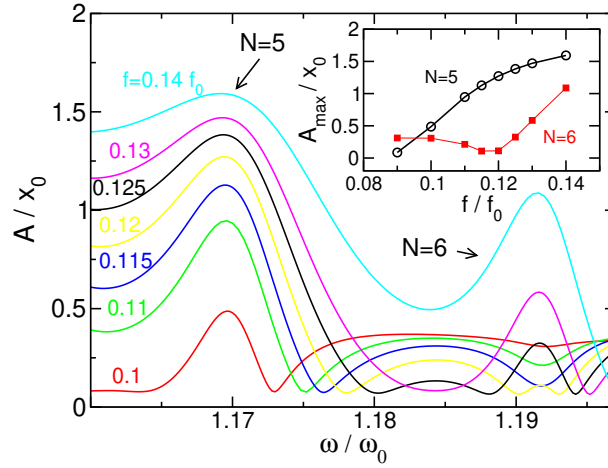


Fig. 4. (Color online) Five- and six-photon resonance of the response curve  $A(x_0)$  for different values of the driving amplitude  $f$ . Inset: Local extremum of the  $N$ -photon resonance for varying driving strength. The six-photon resonance develops from an antiresonance for small driving strengths to a true resonance for larger values of  $f$ . Remaining parameters are  $k_B T = 0.1 \sim 1_0$ ;  $\gamma = 0.1 \sim 1_0$ ;  $\alpha = 0.005 \sim 1_0$ .

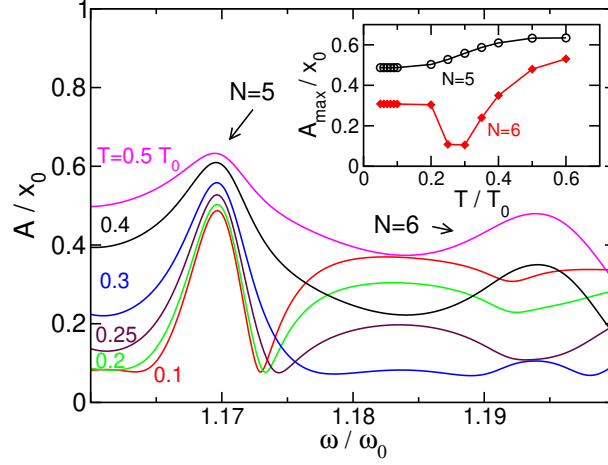


Fig. 5. (Color online) Five- and six-photon resonance of the response curve  $A(\omega)$  for different values of the temperature  $T$ . Inset: Local extremum of the  $N$ -photon resonance for varying temperature. The six-photon resonance develops from an antiresonance for low  $T$  to a true resonance for higher  $T$ . Remaining parameters are  $f = 0.1f_0$ ;  $\gamma = 0.1\gamma_0$ ;  $\epsilon = 0.005\epsilon_0$ .

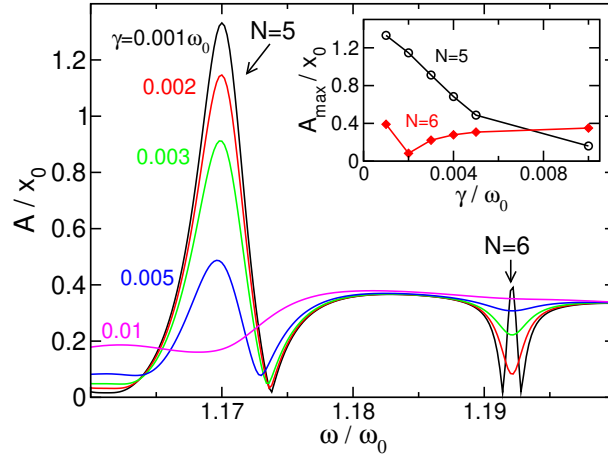


Fig. 6. (Color online) Five- and six-photon resonance of the response curve  $A(\omega)$  for different values of the temperature  $T$ . Inset: Local extremum of the  $N$ -photon resonance for varying temperature. The six-photon resonance develops from an antiresonance for low  $T$  to a true resonance for higher  $T$ . Remaining parameters are  $f = 0.1f_0$ ;  $\gamma = 0.1\gamma_0$ ;  $\epsilon = 0.005\epsilon_0$ .

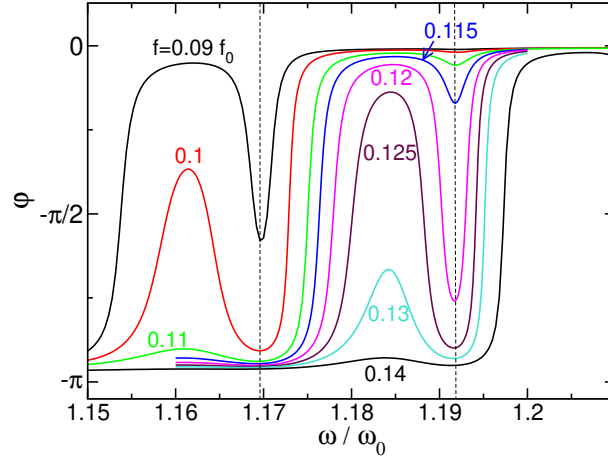


Fig. 7. (Color online) Phase shift  $\Theta$  for the five- and six-photon resonance for different driving amplitudes  $f$ . The dashed vertical lines mark the  $N = 5$  and the  $N = 6$  photon transition. Remaining parameters are  $T = 0.1 T_0$ ;  $\gamma = 0.1 \gamma_0$ ;  $\delta = 0.005 \gamma_0$ .

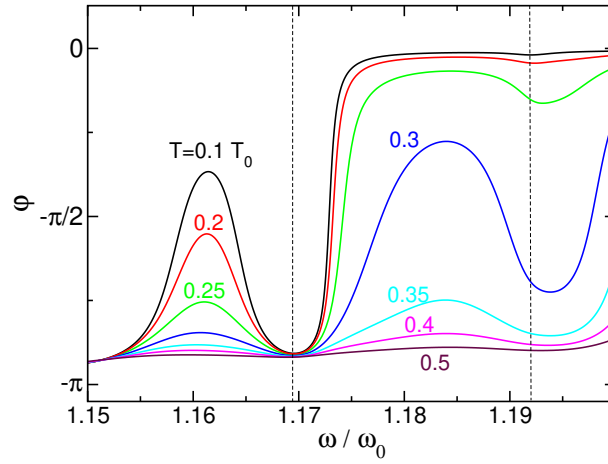


Fig. 8. (Color online) Phase shift  $\Theta$  for different values of the temperature  $T$ . The dashed vertical lines mark the  $N = 5$  and the  $N = 6$  photon transition. Remaining parameters are  $f = 0.1 f_0$ ;  $\gamma = 0.1 \gamma_0$ ;  $\delta = 0.005 \gamma_0$ .

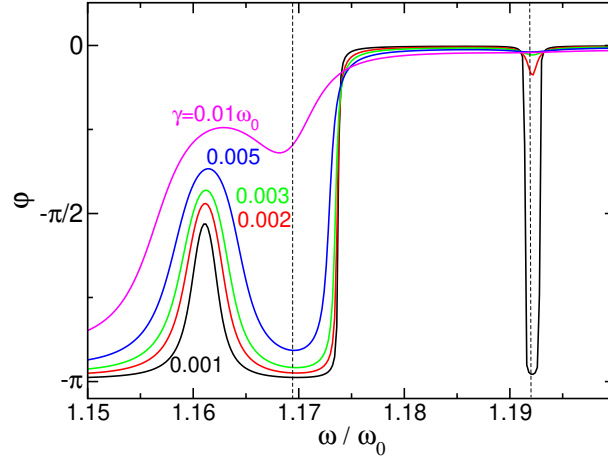


Fig. 9. (Color online) Phase shift  $\phi$  (in radians) for different values of the damping constant  $\gamma$ . The dashed vertical lines mark the  $N = 5$  and the  $N = 6$  photon transition. Remaining parameters are  $f = 0.1f_0$ ;  $\beta = 0.1$ ;  $T = 0.1T_0$ .

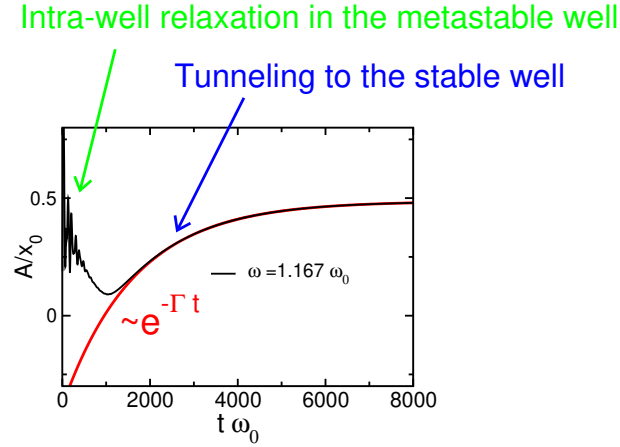


Fig. 10. (Color online) Time-resolved dynamics of  $A$  for  $\omega = 1.167\omega_0$  (black solid line). Fast transient oscillations occur as "intra-well" relaxation in the metastable well. The long-time dynamics is governed by a slow exponential decay to the globally stable state characterized by a rate  $\Gamma$  (tunneling rate). The red solid line shows a fit to an exponential  $e^{-\Gamma t}$ . Here,  $\beta = 0.1$ ;  $f = 0.1f_0$ ;  $k_B T = 0.1T_0$  and  $\gamma = 0.005\omega_0$ .

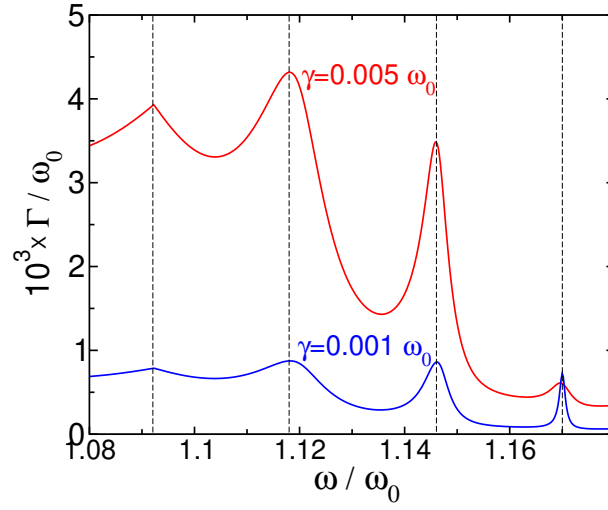


Fig. 11. (Color online) Tunneling rate  $\Gamma$  for the slow dynamics of the amplitude  $A$  for approaching the steady state for two different damping strengths. The peaks correspond to resonant tunneling in the dynamic bistability. Note that tunneling is increased for increasing  $\gamma$  (bath-assisted resonant tunneling). Moreover,  $\gamma = 0.1 \omega_0$ ;  $f = 0.1 f_0$  and  $k_B T = 0.1 \hbar \omega_0$ .